Elastic properties of cellular metals processed by sintering mats of fibres

F. Delannay
Université catholique de Louvain, Département de sciences des matériaux et des procédés, PCIM, Place Sainte Barbe 2, B-1348 Louvain-la-Neuve, Belgium.
T.W. Clyne
University of Cambridge, Department of Materials Science and Metallurgy, Pembroke Street, Cambridge CB2 3QZ, U.K.

Abstract

This work aims at elucidating some basic mechanical properties of cellular-like materials made by sintering mats of continuous metallic fibres. The fibres are 12 μm diameter fibres of stainless steel 316L and the fibre volume fraction in the mat is typically 20%. The random planar orientation of the fibres in the plane of the mat provides transverse isotropy. All five independent elastic constants were measured. The efficiency of the fibre network architecture depends on the average fibre misorientation with respect to the plane of the mat.

1. Introduction

A variety of natural and man-made materials consist of high aspect ratio fibres or continuous fibres assembled by bonds at their contacts points. Common examples are paper, filters, textile felts, glass or ceramic wool plates for thermal insulation, or fibre preforms for composite reinforcement. The mechanical properties of such materials are determined by the properties of the fibres, the fibre volume fraction, the fibre distribution architecture, and the strength of the nodes at fibre contact points. Networks of sintered fibres can be considered as particular cases of cellular materials [1]. It is thus tempting to model the properties of such networks in the framework of the mechanics of three-dimensional cellular solids.

This work aims at characterizing the elastic properties of porous materials made by sintering mats of continuous metallic fibres. The fibres are 12 μm diameter fibres of stainless steel 316L with random planar orientation in the plane of the mat. The advantage of using metallic fibres is that bonding at fibre nodes can be fairly easily obtained by sintering and that, thanks to the ductility of the fibres, the flow strength and stiffness of the mat (in the in-plane and through-the-thickness directions) can be measured over large strain ranges both in tension and in compression. These features will be demonstrated in this paper.

2. Experimental method

The sintered fibre mats were supplied by N.V. Bekaert S.A. They contained 20 vol% of continuous, 12 μm diameter fibres of stainless steel 316L produced by bundle drawing [2, 3]. The method of preparation involves three steps : (1) the making of loose felts of fibres with random planar symmetry by randomly bowing in a plane the continuous fibres produced by bundle drawing ; (2) the stacking of these felts upon one another and the compression of the stack to a plate with a fibre volume fraction $V_f = 20 \pm 1$ % ; (3) the sintering of the plate under protective atmosphere in conditions optimised for providing the highest strength to the

J. Banhart, M.F. Ashby, N.A. Fleck: *Metal Foams and Porous Metal Structures.* © MIT Verlag (1999)

mat. SEM observation shows that, after sintering, crossing fibres are completely welded at all contact points : the size of the contact "neck" is approximately equal to the fibre diameter. These materials are widely used as filters in the chemical industry. They have recently been used for reinforcing Al alloys [4]. The thickness of the plates investigated in this work was 10 mm. The specimens for mechanical testing were machined by spark erosion. The initial fibre volume fraction V_f was determined by weighing.

The mats present transverse isotropy. Their elastic properties are thus characterised by 5 independent elastic constants. In order to obtain the whole set of elastic constants, different testing methods were used depending on the loading direction : in-plane (plane x_1, x_2) and through-the-thickness (x_3).

In-plane properties were measured only in tension. The specimens were cuboid bars of size 70 x 14 x 10 mm (in the x_1, x_2, and x_3 directions, respectively). The ends of the bars were infiltrated with epoxy resin on a length of about 1 cm in order to allow the specimens to be held in the grips of the testing machine. Two clip-gauge extensometers were used for measuring simultaneously the longitudinal in-plane engineering strain ε_{11} and either the transverse engineering strain ε_{22}, or the transverse engineering strain ε_{33}, depending on the test. The strain rate was about 0.3×10^{-2} min^{-1}. The three elastic constants E_1, ν_{12}, and ν_{13} were measured by reversing repeatedly the straining rate during the tests. The reproducibility was assessed by carrying out four tests, i.e. two tests for each measurement of ε_{22} and ε_{33}. The discrepancy between the tests was very small. No significant strain rate dependence was observed.

The mats were also tested in tension and compression along direction x_3 perpendicular to the plate. The specimens were disks of 10mm height (i.e. the plate thickness). Tests were made on disks with three different diameters : 20 mm, 14 mm and 8 mm. The disks were merely glued on the specimen holder using an epoxy adhesive. The amount of epoxy being low, the depth of penetration of epoxy into the mat was estimated to be less than 0.3 mm. The strain, averaged on the whole height of the disk, was measured by means of a LVDT sensor. The Poisson ratio ν_{31} was not measured (ν_{31} will be deduced from the measured values of E_3, E_1, and ν_{13}).

The torsion tests were made in a torsion testing machine by twisting along the x_3-direction. The torque deflection was measured with a LVDT. The specimen diameter was 14 mm. The machine allowed control of both the torque and the longitudinal load; the longitudinal load was dynamically regulated at zero all during the torsion test. The torsion rate was about 1 degree min^{-1}.

3. Results

3.1. In-plane properties

Figure 1 shows the engineering stress-strain curves for one of the two tests involving the measurement of ε_{11} and ε_{33}. The yield strength $\sigma_{0.2\%}$ is 11 MPa. A fairly linear strain hardening is observed until fracture. Depending on the test, tensile fracture occurred at an engineering strain of 10 ± 2 % and the tensile strength σ_u was equal to 19 ± 1 MPa.

Quite strikingly, the transverse strain ε_{33} is positive, and of the same order of magnitude as the longitudinal strain ε_{11}. The plastic Poisson "contraction" - $(\varepsilon_{33}/\varepsilon_{11})_{pl}$ (ratio of the plastic components of the transverse and longitudinal strains) in the range $1\ \% < e_{11} < 7\ \%$ is equal to - 0.87 ! (As shown hereafter, a negative plastic Poisson strain $\varepsilon_{11}/\varepsilon_{33}$ was also observed during the out-of-plane tests). The tests involving the measurement of ε_{11} and ε_{22} showed

that the transverse strain ε_{22} is negative, and much smaller than the longitudinal strain : the the ratio - $(\varepsilon_{22}/\varepsilon_{11})_{pl}$ in the range 1 % < e_{11} < 7 % is equal to 0.27. Combining these two results, one derives that in-plane plastic straining involves a volume expansion of the mat : $[\Delta V/(V\Delta e_{11})]_{pl}$ = 1.6 (i.e. 10% plastic strain induces 16% volume expansion).

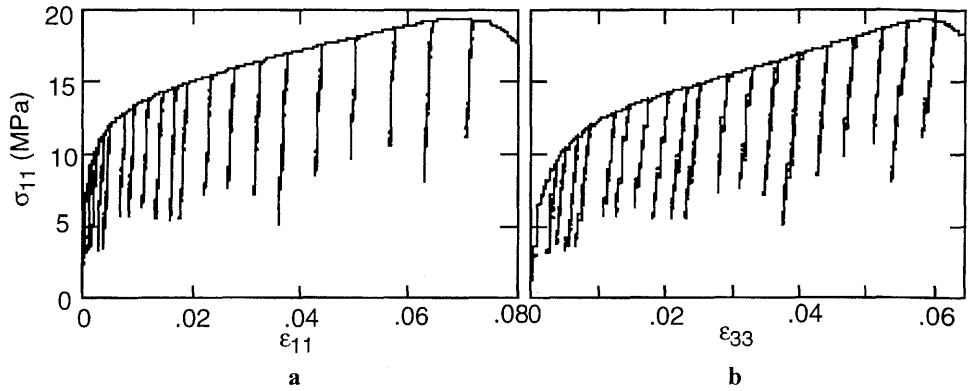

Figure 1 : Engineering stress-strain curves σ_{11}-ε_{11} (a) and σ_{11}-ε_{33} (b) recorded simultaneously during in-plane tensile testing

Figure 2a shows the variation of the Young's modulus E_1 as a function of ε_{11} measured from the slopes of the successive unloading lines for two different σ_{11}-ε_{11} curves similar to Fig. 1.a. The discrepancy between the two tests is small. E_1 does not change much with plastic straining : it remains mostly equal to $E_1 \approx 7.5 \pm 1$ GPa. Figure 2b shows the variation of the Poisson ratios ν_{12} and ν_{13} measured from the slopes of the successive unloading lines in curves such as Fig. 1.b. ν_{12} appears to decrease from about 0.4 at the beginning of the test to a plateau value at about 0.25. ν_{13} is large and negative : it remains approximately constant at $\nu_{13} \approx$ - 1.7 independently of the strain.

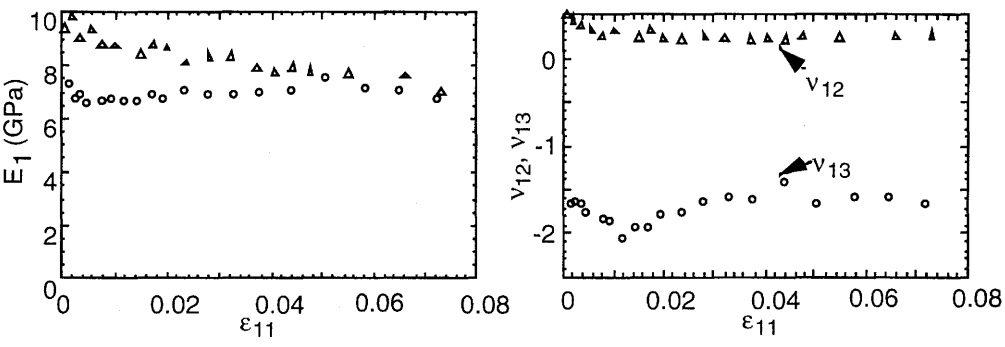

Figure 2 : Variation of (a) the in-plane Young's modulus E_1 and (b) the Poisson ratios ν_{12} and ν_{13} as a function of ε_{11}

3.2. Out-of-plane properties

Compression along x_3 was tested using a specimen disk diameter of 20 mm. The strain rate was of the order of 0.1 min^{-1}. No significant strain rate dependence was observed. The

change of the Young's modulus E_3 as a function of the strain was measured by reversing the straining rate at successive intervals. As some strain hysteresis was observed when unloading to zero load, E_3 was measured from the σ-ε slope at the beginning of each unloading step. The specimen appeared to deform very uniformly and the test was stopped when the height of the specimen had been reduced from 10 mm to 5.3 mm, which corresponds to a total true strain $\varepsilon_{33} = -0.6$. The diameter of the specimen had hardly changed after the test : actually, a slight contraction was measured, which corresponded to a total strain $\varepsilon_{11} \approx -0.6 \times 10^{-2}$. Assuming $\varepsilon_{11} = 0$, the longitudinal strain ε_{33} could be straightforwardly converted into a change of the fibre volume fraction V_f.

Figures 3a and 3b present the variation of the flow strength σ_{33flow} and of the modulus E_3, respectively, as a function of the fibre volume fraction V_f. The first V_f value at which the Young's modulus could be measured was 0.215, which corresponds to a strain $\varepsilon_{33} = 2.x\ 10^{-2}$. The initial values of σ_{33flow} and E_3 at this V_f were 1.7 MPa and 0.22 GPa, respectively. With respect to the Young's modulus E_S of the fibres, this corresponds thus to $E_3/E_S = 10^{-3}$.

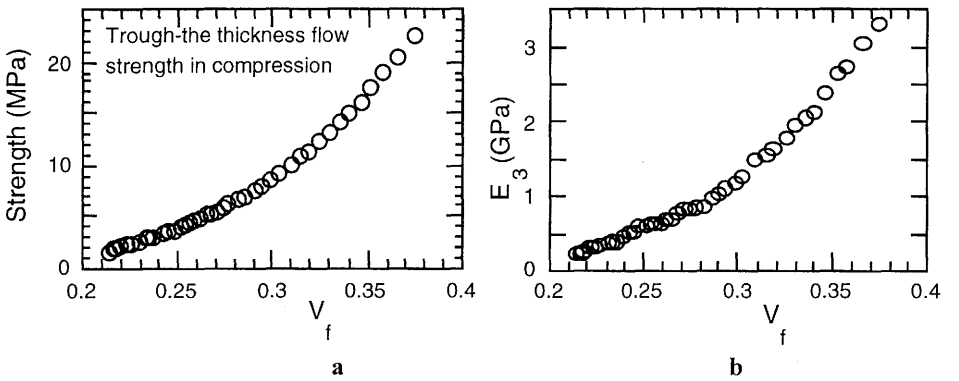

Figure 3 : Variation of (a) the flow strength σ_{33flow} and (b) the modulus E_3 as a function of the fibre volume fraction V_f during a compression test

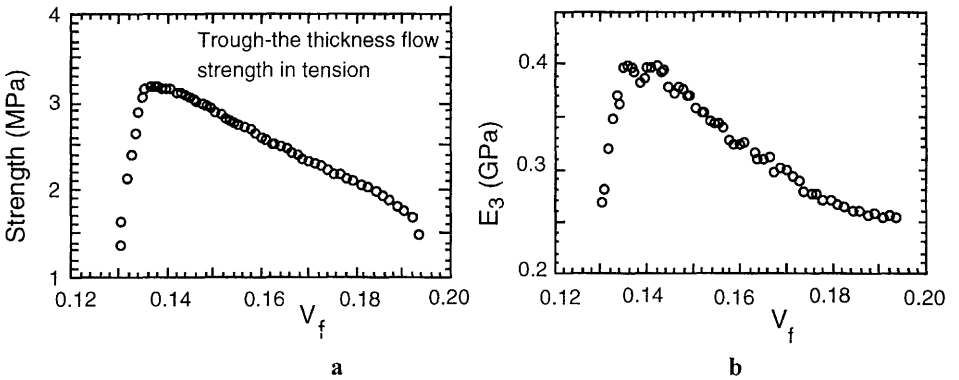

Figure 4 : Variation of (a) the flow strength σ_{33flow} and (b) the modulus E_3 as a function of the fibre volume fraction V_f during a tension test

Tensile tests along the x_3-direction confirmed the results of the compression tests. Deformation appeared again very uniform all along the specimen height. The fracture strain was large: depending of the test, the total true strain $\varepsilon_{33fract}$ amounted to about 0.3. The

specimen diameter hardly changed until fracture : measurement of the diameter after testing indicated a total reduction of the cross section area ($\varepsilon_{11fract}^2$) by 2 ± 0.5 %. The longitudinal strain ε_{33} could thus again be straightforwardly converted into a change of the fibre volume fraction V_f by assuming $\varepsilon_{11} = 0$. Figure 4a and 4b present the variation of the flow strength σ_{33flow} and of the modulus E_3, respectively, as a function of the fibre volume fraction V_f during a tension test along the x_3-direction. At $V_f = 0.19$, the initial value $\sigma_{33flow} = 1.6$ MPa very well agrees with the value measured in compression. The initial value $E_3 \approx 0.26$ GPa also agrees with the initial E_3 value measured in compression. Interestingly, the Young's modulus increases with increasing tensile straining, i. e. with decreasing fibre volume fraction.

The evolution of the shear modulus G_{13} was measured by repeatedly reversing the torsion rate during the torsion test. As a torsion test does not lead to fracture, the test was interrupted after a sufficient plastic deflection had been reached and a tensile test was carried out (under zero torque) directly on the same torsion machine without having to ungrip the specimen. It was verified that no measurable transverse deformation ε_{33} had occurred during the torsion test. The shear strain γ_{13} in torsion increases linearly from the rod axis to the surface whereas the increase of the shear stress τ_{13} is non-linear in the plastic regime. In order to present the data in a sensible way, we express the data as a function of the shear strain at the surface whereas the shear strength is expressed as an equivalent shear stress, $\tau_{13equ} = 16\ T/\pi\ D^3$, where T is the measured torque and D is the specimen diameter. τ_{13equ} is the shear stress that would exist at the specimen surface in the purely elastic case. In the plastic regime, this equivalent stress is larger than the average shear stress in the specimen.

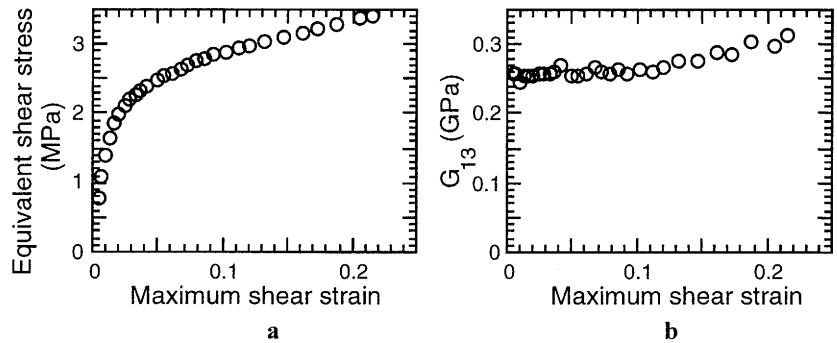

Figure 5 : Variation of (a) the equivalent shear strength in torsion and (b) the shear modulus G_{13} as a function of the shear strain at the surface of the specimen disk

Figure 5a presents the variation of this equivalent shear strength as a function of the maximum (i.e. surface) shear strain. The torsion deformation was very uniform in the specimen. The shear flow strength is comparable to the transverse flow strength in compression and in tension. The test was interrupted when the surface shear strain had reached 0.22. Figure 5b shows the variation of the shear modulus G_{13} as a function of the surface shear strain. One notices only a slight increase with increasing deformation. The initial value $G_{13} = 0.26$ GPa is similar to the value $E_3 = 0.22$ GPa measured in compression.

4. Discussion

As summarised in Table 1, the tests provide all five independent elastic moduli of a sintered mat with 20% volume fraction of fibres. Using the reciprocal relation $E_1\nu_{31} = E_3\nu_{13}$, one

deduces $\nu_{31} = -3.4 \times 10^{-2}$ for $V_f = 0.2$ (i.e. $\nu_{31} \approx 0$ for all practical purposes). In addition, we can calculate, for transverse isotropy, $G_{12} = E_1/[2(1 - \nu_{12})]$.

Table 1 : Elastic constants of a cellular metal with 20 vol % stainless steel fibres

$E_1 = E_2$	$\approx$ 7.5 GPa
E_3	$\approx$ 0.2 GPa
$G_{13} = G_{13}$	$\approx$ 0.25 GPa
G_{12}	$\approx$ 5 GPa
ν_{12}	$\approx$ 0.25
ν_{13}	$\approx$ - 1.7
ν_{31}	$\approx$ 0

As noted by Gibson and Ashby [1], as the cell edges are loaded primarily in bending, the stiffness of an open-celled foam should scale with V_f^2. The present results can thus be better appreciated by the ratio $(E_{mat}/E_s)/V_f^2$. For the in-plane modulus, this translates into $E_1/E_s = 0.87\ V_f^2$, which is close to the value expected for an ideal foam [1]. The initial value of the through-the-thickness modulus, translates into $E_3/E_s = 2.2\ 10^{-2}\ V_f^2$. However, at the end of the compression test E_3 has reached 3.3 GPa for a volume fraction of = 0.375, i.e. $E_3/E_s = 0.11\ V_f^2$. This indicates that the enhancement of the trough-the-thickness stiffness is much larger than the mere effect of the change of V_f. The improvement of the efficiency of the fibre network architecture with respect to stiffness is even more significant during transverse tension : for a 20 mm diameter specimen for example, the ratio E_3/E_s increases from $E_3/E_s = 3.3\ 10^{-2}\ V_f^2$ at $V_f = 0.19$ to $E_3/E_s = 9.5\ 10^{-2}\ V_f^2$ at $V_f = 0.14$. Accounting for the change of V_f shows that this change is quite more significant than it appears on the graph : for the 20 mm diameter specimen for example, the ratio E_3/E_s increases from $E_3/E_s = 3.3\ 10^{-2}\ V_f^2$ at $V_f = 0.19$ to $E_3/E_s = 9.5\ 10^{-2}\ V_f^2$ at $V_f = 0.14$.

A model for predicting the variation of the elastic constants of a fibre mat as a function of fibre volume fraction and fibre orientation has been developed [5]. This model suggests how, for a given fibre volume fraction, the stiffness and elastic anisotropy are determined by the average misorientation of the fibres with respect to the plane of the mat. Hence, this work opens some clues for designing the architecture of a sintered fibre mat according to the elastic properties required for a particular structural application.

Acknowledgments
The authors are indebted to C. Salmon, M. Sinnaeve, and L. Tao for help in carrying out the tests. The fibre mats were supplied by N.V. Bekaert S.A.. Financial support of the British Council and of SSTC (Belgium) in the framework of program PAI 41 is gratefully acknowledged.

References

[1] L.J. Gibson and M.F. Ashby, Cellular solids, Cambridge University Press, 1997
[2] S.J. Everett : US Patent 2050298, 1936
[3] R. De Bruyne: Advances in Powder Metallurgy and Particulate Materials, 1996, vol 5, pp. 16-99
[4] F. Boland, C. Colin, C. Salmon, and F. Delannay, Acta Mater. 46 (1998) 6311-23
[5] F. Delannay, in preparation